Sources, variability and fate of freshwater in the Bellingshausen Sea, Antarctica

Heather C. Regan[a,b], Paul R. Holland[a], Michael P. Meredith[a], Jennifer Pike[b]

[a] *British Antarctic Survey, Cambridge, United Kingdom.*
[b] *School of Earth and Ocean Sciences, Cardiff University, United Kingdom.*

Abstract

During the second half of the twentieth century, the Antarctic Peninsula was subjected to a rapid increase in air temperatures. This was accompanied by a reduction in sea ice extent, increased precipitation and a dramatic retreat of glaciers associated with an increase in heat flux from deep ocean water masses. Isotopic tracers have been used previously to investigate the relative importance of the different freshwater sources to the adjacent Bellingshausen Sea (BS), but the data coverage is strongly biased toward summer. Here we use a regional model to investigate the ocean's response to the observed changes in its different freshwater inputs (sea ice melt/freeze, precipitation, evaporation, iceberg/glacier melt, and ice shelf melt). The model successfully recreates BS water masses and performs well against available freshwater data. By tracing the sources and pathways of the individual components of the freshwater budget, we find that sea ice dominates seasonal changes in the total freshwater content and flux, but all sources make a comparable contribution to the annual-mean. Interannual variability is dominated by sea ice and precipitation. Decadal trends in the salinity and stratification of the ocean are investigated, and a 20-year surface freshening from 1992-2011

is found to be predominantly driven by decreasing autumn sea ice growth. These findings will help to elucidate the role of freshwater in driving circulation and water column structure changes in this climatically-sensitive region.

Keywords: Bellingshausen Sea, Antarctica, Freshwater, Tracers, Sea ice trends

1. Introduction

From the 1950s until the late 1990s the Antarctic Peninsula (AP) warmed more rapidly than any other region in the Southern Hemisphere, with air temperatures increasing by nearly 3°C, though recent changes in wind patterns may have led to a pause of the warming (Turner et al., 2016). Over the same period, the summer surface ocean in the adjacent Bellingshausen Sea (BS) warmed and salinified (Meredith and King, 2005). Unlike elsewhere in Antarctica, the Bellingshausen and Amundsen seas have seen an overall decrease in sea ice duration (Stammerjohn et al., 2012) and extent (Parkinson and Cavalieri, 2012) over the satellite era, with changes focussed on the summer (Holland, 2014). Furthermore, along the AP, 87% of glaciers have retreated since records began (Cook et al., 2005), with mass loss (Wouters et al., 2015) and thinning (Paolo et al., 2015) observed in the southern BS ice shelves. While atmospheric circulation changes and warming are thought to be drivers, they cannot fully explain the ice loss, and recent indications are that the ocean is playing an important role (Wouters et al., 2015; Cook et al., 2016).

The BS can be characterised as being comprised of three water masses.

Below the permanent pycnocline, which is around 150-200 m on the shelf, intrusions of Circumpolar Deep Water (CDW) from the Antarctic Circumpolar Current (ACC) onto the shelf provide a source of heat and salt, with the onshelf flow being especially effective within glacially-scoured canyons that cross the shelf (e.g. Zhang et al. (2016), Klinck et al. (2004), Graham et al. (2016)). In the northern BS the CDW layer has thickened and warmed in recent decades (Martinson et al., 2008). This deep layer is overlain by cool, fresh Antarctic Surface Water (AASW), which forms a homogeneous layer around 50-150 m thick in winter, but which is capped in summer by a relatively thin layer that is warmed by insolation and freshened by diverse freshwater inputs. The subsurface temperature minimum that is created reflects the previous winter's mixed layer, and hence is termed Winter Water (WW) (Klinck et al., 2004).

The freshwater balance of the BS is important because salinity controls density in polar waters as thermal effects on density are small (e.g. Talley (2011), chapter 3), and therefore strongly affects ocean circulation and mixing. It has been argued that cyclonic circulation on the shelf is amplified by freshwater-induced buoyancy effects (Savidge and Amft, 2009), and a summer coastal current on the BS shelf is driven at least partially by glacial melt and precipitation (Moffat et al., 2008). Sea ice melting and freezing, and freshwater from meteoric sources (precipitation and evaporation, and the melting of ice shelves, icebergs, and glacier fronts) may all contribute significantly to the mean freshwater balance of the BS and its seasonality.

Increases in both precipitation days (Turner et al., 2005b) and snowfall accumulation over longer timescales (Thomas et al., 2008) to the Antarctic

Peninsula suggest an increase in precipitation freshwater, particularly since 1950. This, along with the extensive retreat of glaciers in recent decades are concurrent with increased calving ice and surface freshwater input into the ocean. The potential consequences range from seasonal effects altering ocean currents and stratification in summer, to influencing the formation of sea ice in winter via surface ocean temperature changes and snow flooding. Sea ice production may be enhanced by an increase in stratification that reduces the oceanic heat flux from below (Hellmer, 2004). There are also important biological consequences, as more glacial meltwater can enhance water column stability and nutrient provision, favouring phytoplankton blooms (Dierssen et al., 2002).

Basal melting of ice shelves varies significantly due to changes in the CDW layer and wind strength (Holland et al., 2010; Dinniman et al., 2012), but appears to have increased overall in the BS region (Paolo et al., 2015; Wouters et al., 2015), causing ice-shelf thinning and increased meltwater input into the ocean. This can cause numerous feedbacks, including stabilisation (Hellmer, 2004) or destabilisation (Merino et al., 2016) of the water column depending upon the depth of meltwater injection, and intensification of coastal currents (Nakayama et al., 2014).

The reduction in BS sea ice extent and duration, with an increased spring meltwater flux (Holland, 2014), has a variety of effects. Reduced summer sea ice cover can increase autumn ice production rates by exposing a greater area of surface water to the atmosphere (Meredith et al., 2010). It can also change basal melt rates of ice shelves (Holland et al., 2010) by altering stratification and therefore the vertical flux of heat from CDW through the water column.

Given the strong climatic changes in the BS region in recent years, there is a need to better understand the functional response of the different freshwater components to changing forcings so that their individual and collective impacts on circulation, climate and the ecosystem can be determined and better predicted.

There are a number of observations available to assist in closing the freshwater budget, though whilst spatial and temporal coverage is more complete here than in any other region of the Southern Ocean, it is still strongly biased toward the summer season. In combination with salinity measurements, oxygen isotope (δ^{18}O) measurements can separate meteoric freshwater inputs from sea ice melt (Meredith et al., 2008), though further deducing contributions from each meteoric sink and source is not possible by this method. Measurements in the northern BS show a general dominance of meteoric water in coastal areas, though years of weak precipitation and/or extreme sea ice can show comparable quantities of sea ice melt (Meredith et al., 2016). Over time there has been a decline in meteoric water in the surface waters adjacent to Adelaide Island, north of Marguerite Bay, due to deepening winter mixed layers (Meredith et al., 2013). This is despite increased glacial discharge (Pritchard and Vaughan, 2007) and snowfall (Thomas et al., 2008) in the BS. However, interannual variability in freshwater inputs from different sources and strong regional structure in their injection locations can complicate the interpretation of data on wider temporal and spatial scales (Meredith et al., 2016), highlighting the importance of understanding the three-dimensional spatial variance of freshwater composition over time.

Oxygen isotope measurements can also provide palaeoceanographic infor-

mation relating to the freshwater content of the water column at particular locations. At Palmer Deep in the northern peninsula, Pike et al. (2013) attribute lowering of δ^{18}O in the early Holocene to increased glacial discharge coinciding with warming air and sea surface temperatures and ice sheet retreat and thinning, with increased insolation and La Niña events being stronger contributors to warmer temperatures. The method of combining the measurements with known preferences of different diatom species can also be used to investigate seasonal variations in the context of CDW inflow; for example, Swann et al. (2013) found larger seasonality during deglaciation than present-day, attributed to retreat of ice sheets. However, challenges remain with regard to fully ascribing the meteoric water content changes to glacial melt versus precipitation.

Overall, although the freshwater system of the BS is arguably better measured and understood than most other Southern Ocean regions, there is still insufficient knowledge given its climatic, cryospheric and ecological importance. Here we use a regional ocean model to investigate the spatial and temporal variations in freshwater sources - sea ice melt/freeze, precipitation/evaporation, iceberg melt, ice shelf melt and glacier melt - and their fate in the BS in recent decades. By using passive tracers in the model, we assess the freshwater balance of the BS by quantifying each freshwater component and its pathways across the shelf. This provides unique insights into the regional freshwater budget, which may be used to consider the ocean's role in sea ice loss and glacial ice retreat in the region.

2. Materials and Methods

2.1. Model Overview

The Massachusetts Institute of Technology general circulation model (MITgcm) is used, generally following the configuration of Holland et al. (2014), with the same sea ice and ice shelf components and horizontal and vertical tracer diffusion schemes. Here the horizontal resolution is set to 0.2°, providing an isotropic grid spacing of 6 km in the south and 13 km in the north of the model domain. The model uses a z-level coordinate system with 50 levels, with a vertical resolution varying from 10 m spacing in the top 100 m to over 400 m spacing in the deep ocean, to handle surface freshwater inputs and also ice shelf melting at depth on the shelf. To account for complex topography the model uses partial cells, with a minimum open cell fraction of 0.25. The model domain covers the area from 74.4-55 °S and 95-55 °W (Figure 1). This area extends beyond the shelf break and includes the Antarctic Circumpolar Current (ACC), important due to its influence on shelf processes.

[Figure 1 about here.]

The ocean boundaries are forced with the 1990-1999 monthly climatological ocean temperature, salinity, and velocities and sea ice area, thickness and velocities of Holland et al. (2014). We have deliberately chosen this time period from their model as it is the first 10 years after spin-up, so provides a realistic state. We do not use a timeseries for boundary conditions as we are only studying local trends. Sea ice velocities are not prescribed at the boundary if the model predicts ice exiting the domain, to avoid unphysical ice convergence. The run uses BEDMAP2 bathymetry and ice shelf cavities (Fretwell et al., 2013), with any ice shelf thinner than 10 m removed.

The model was run from 1979 to the end of 2014 using the climatology of World Ocean Atlas 2005 as initial conditions, with results presented from 1989 onwards to allow for 10 years of model spin-up time. All atmospheric forcing variables are provided from the 0.75° resolution ERA-Interim reanalyses (Dee et al., 2011) at 6-hourly resolution. There is no tidal forcing in the model.

2.2. Glacial Inputs

The ice-shelf melting parameterisation follows De Rydt et al. (2014) so that the melting is dependent on both thermal and haline driving and velocity. All parameters are taken from Holland and Jenkins (1999), apart from the drag coefficient, $c_d = 0.001$, which we tuned from 0.0015 over successive runs so that the modelled melt rate of George VI Ice Shelf (GVIIS) was consistent with observations (section 3.1).

The remaining external freshwater inputs are iceberg melting, glacier-front melting, and freshwater runoff. These inputs are collectively represented by a prescribed surface freshwater flux field. Liquid glacier-surface runoff is negligible (van Wessem et al., 2016), and ocean melting at the front of glaciers is taken to be small compared with the calving and subsequent melt of icebergs. Therefore we refer to these terms collectively as iceberg melt, though a fraction may come from ice front melting. Note also that, in reality, iceberg and ice-front meltwater is released at depth, not at the surface, and that this melting entails a consumption of latent heat; neither effect is included in the model, though they may not be insignificant.

There are few data available to guide the choice of the prescribed iceberg melting field. There is modelling and observational evidence to suggest that

the freshwater contribution from iceberg melt is localised, with no strong advection of icebergs into or out of the region (Tournadre et al., 2015; Merino et al., 2016), so we adopt the hypothesis that iceberg melting is concentrated close to the southern coastline and is similar in magnitude to local glacial discharge. We assign a flux of 130 Gt/year, calculated from the sum of glacial discharge of each basin along the northwest side of the peninsula found by van Wessem et al. (2016). We distribute this total flux uniformly along the western peninsula coast, concentrated inshore and decreasing linearly to zero 100 km offshore (Dierssen et al., 2002), and uniformly with time in the absence of other data. Both the peak freshwater flux and distribution compare reasonably well with Merino et al. (2016) along a large portion of the peninsula, with slight overestimations in the north.

The sensitivity of the results to these assumptions was tested by altering the magnitude of the total flux, extending the flux further offshore, and randomly redistributing the field to disrupt the spatial pattern. While the magnitude of the resulting freshwater content is altered, its spatial variability does not change. Interannual variability of fluxes are slightly varied due to the additional surface freshwater, but trends in total freshwater content remain similar. Thus whilst this prescription necessarily involves assumptions concerning the spatial and temporal injection of freshwater to the ocean, in the absence of more fully constrained observational fields it is the best that can be achieved.

2.3. Tracers

To determine the extent and nature of the influence of different sources of freshwater, the MITgcm code was developed so that tracing multiple fresh-

water tracers from tagged sources (sea ice, precipitation, evaporation, iceberg melt, and ice shelf meltwater input) is possible, including ice shelf melting at depth. The sea ice freshwater source/sink includes the effects of melting, freezing, and flooding of ice-borne snow. Precipitation and evaporation are dealt with separately because both have a different origin and sensitivity, and both are handled differently in the model.

The standard code allows a passive tracer to be enhanced or diminished by the total surface freshwater flux according to

$$\frac{\Delta\phi}{\Delta t} = \frac{F(\phi_S - \phi)}{\Delta z} \tag{1}$$

where ϕ is the concentration of tracer in the ocean, ϕ_S is the concentration of tracer in the freshwater, F is the volume flux of freshwater in m/s, defined positive downwards, and Δz and Δt are the top grid cell thickness and time step. This expression is valid provided that the freshwater is also added as a material volume flux to the top grid cell. Tracers are subsequently advected and diffused in the same way as heat and salt.

Assuming a constant flux and source concentration of a single tracer, the solution to (1) is

$$\phi = \phi_S(1 - e^{\frac{-Ft}{\Delta z}}) \tag{2}$$

This demonstrates that the tracer concentration cannot exceed ϕ_S if the surface flux is positive (a source), but can become arbitrarily negative relative to the initial tracer concentration if the surface flux is a sink. For example, if sea ice grows more than it melts the water becomes saltier, and a negative sea ice freshwater tracer concentration is left behind.

The MITgcm code adaptation for tagging freshwater sources involves additional complexity because fluxes of freshwater from other sources dilute

the tracer of the source in question simply by adding additional volume to the ocean that is devoid of that tracer. For example, the formulation for tracers ϕ_1 and ϕ_2 with source concentrations ϕ_{S_1} and ϕ_{S_2} and fluxes F_1 and F_2 respectively is

$$\frac{\Delta\phi_1}{\Delta t} = \frac{1}{\Delta z}(F_1(\phi_{S_1} - \phi_1) - F_2\phi_1) \tag{3}$$

$$\frac{\Delta\phi_2}{\Delta t} = \frac{1}{\Delta z}(F_2(\phi_{S_2} - \phi_2) - F_1\phi_2) \tag{4}$$

As such, a particular tracer concentration in any given grid cell is affected by the fluxes of all tracers, but only the concentration of the relevant source.

In this study we trace a total of 6 freshwater sources: sea ice melt/freeze, precipitation, evaporation, iceberg melt, ice shelf melt, and a tracer of the total freshwater source. We set the initial concentration of all tracers to be 0, and then allow them to evolve to represent the contribution from freshwater sources, which are set to a tracer value of 1 for each source. A seasonally varying quasi-steady state is obtained when the local tracer sources and sinks are balanced by the lateral fluxes of tracer out of the domain, which occurs within the model spin-up period. All tracers are set to zero on boundary inflows, i.e. we are only tracing locally-sourced freshwater. Further information can be found in Regan (2017).

3. Climatological results

3.1. Model validation

[Figure 2 about here.]

Figure 2 shows the mean climatological bottom potential temperature and salinity for the period 1989-2014 inclusive, along with winter (July-September)

sea ice thickness, concentration, and drift. The west Antarctic Peninsula shelf is fresher and warmer than the deep waters of the ACC, reflecting the fact that it has shallower bathymetry. Warmer, saline waters fill bathymetric troughs and canyons, highlighting areas where CDW intrudes onto the shelf from the ACC. Shallow areas immediately adjacent to the coast are colder and fresher, reflecting the depth-variation in the water-column properties. Model resolution is important for allowing CDW onto the shelf (Graham et al., 2016), but while temperatures are slightly lower than core CDW temperatures, there is little deviation from the World Ocean Atlas fields that were used to initialise the model, showing that a suitable model climatology is achieved for the purpose of this study.

Crucially for this study, comparisons with CTD profiles are able to validate the salinity and freshwater content. Figure 3 shows the vertical profiles of salinity and derived sea ice melt and meteoric water content of location 65°52.6' S, 68°10.0' W (Figure 1, location P) reproduced from Meredith et al. (2016), along with the associated model output. The general behaviour of each field is captured. Temperature data are much more commonly available, so we compare our model to the World Ocean Atlas. In both the model and observations, most variation in salinity and freshwater content is seen in the top 50 metres of the water column (Figure 3) , though the mixed layer signal in temperature is shallower in the model. The model underpredicts meteoric water content in the top 50 metres, and generally over-predicts sea ice meltwater at the surface. At depth there is a net loss of sea ice meltwater in most years which the model is able to recreate successfully, though the interannual variability in the model at depth is less than in observations. The

model successfully estimates high sea ice melt and fresher waters in 2014, though 2011 and 2012 are less comparable, with observed negative sea ice content not modelled. Overall, the comparison is encouraging considering the difficulties inherent in modelling specific events using reanalysis forcing and relatively coarse model resolution, which are expected to produce less variability.

[Figure 3 about here.]

The modelled sea ice can be compared with satellite observations of ice concentration and drift (e.g. Holland and Kimura, 2016) and thickness (e.g. Xie et al., 2013). The wintertime ice concentration is in good agreement with observations, though the summer ice cover is too low (section 4.2). Modelled ice drift accurately captures the eastward ice current to the north and westward coastal current (not shown in the north due to vector resolution). Modelled ice thicknesses are realistic, with thicker ice near Wilkins and Abbot ice shelves (locations shown in Figure 1).

An assessment of the modelled ice shelf melt flux is an important requirement of this study. Table 1 summarises the six main ice shelves in the domain and their melt rates derived from both the model and glaciological mass budgets. Note that Abbot Ice Shelf is only partially covered by the model. George VI Ice Shelf (GVIIS) is the only ice shelf where there are additional data from oceanographic observations, summarised in Holland et al. (2010). The modelled GVIIS melting (4.74$\pm$0.19 m/yr) is within 3-5 m/yr, the range quoted by Jenkins and Jacobs (2008), but slightly higher than the values found by both Rignot et al. (2013) (3.8$\pm$0.7 m/yr) and Depoorter et al. (2013) (2.88$\pm$0.83 m/yr). Wilkins and Abbot ice shelf melt rates are

within error bars of the latter two studies but Bach, Stange and Venable melt rates are all significantly underestimated by the model. Relatively low model resolution and poorly-known ice-shelf cavity geometry are significant limiting factors and therefore we would not expect to be able to fully recreate ice shelf melt rates in these smaller, poorly sampled cavities, and as such we do not place much faith in their modelled melting. Future improvements to the model can be made once suitable surveys of the cavities have been conducted. Further model validation is provided in Regan (2017).

[Table 1 about here.]

3.2. Freshwater climatology

[Figure 4 about here.]

In the long-term mean, each climatological freshwater source into the Bellingshausen Sea is of comparable magnitude (Figure 4, Table 2), albeit with strong spatial variation. In particular, there is a clear difference between the north and south, separated by Alexander Island and GVIIS. In the north, there is a strong positive contribution of freshwater extending across the shelf break out into the ACC, comprising precipitation, sea ice melt, and imposed iceberg melt. Strong sea ice freezing results in a net loss of sea ice freshwater directly adjacent to the entire coastline. This is particularly apparent in the south, where it is only countered by ice shelf melt and imposed iceberg melt; the cooler climate reduces both the precipitation rate and the open ocean area into which it falls.

[Figure 5 about here.]

The surface tracer concentration fields (Figure 5) reflect the spatial distribution in freshwater fluxes, their relative magnitudes, and redistribution and mixing of the freshwater by ocean processes, and demonstrate that the freshwater composition in any particular location cannot in general be deduced from fluxes alone (or vice versa). Over the deep ocean, evaporation, precipitation, and sea ice melt dominate the total freshwater budget. On the western AP shelf all components have localised contributions, resulting in total freshwater content exceeding 3% concentration in coastal areas and 5% in Marguerite Bay. Evaporation and precipitation demonstrate the role of westward advection along the coastal current from their source regions in the north.

Sea ice meltwater accumulates in the far west despite this being a region of net freezing (Figure 5e). Adjacent to this sea ice meltwater lies a pool of water depleted in sea ice tracer at the surface, due to strong ice growth in polynyas in Eltanin Bay (Holland et al., 2010). This is countered by meteoric freshwater to result in a net positive concentration of freshwater tracer overall, masking the sea ice signal, which reaffirms the need to consider the behaviour of individual freshwater components. All tracer concentrations are elevated east of Ronne Entrance, particularly in Marguerite Bay. Ice shelf melt reaches the surface in large volumes in Marguerite Bay but not elsewhere.

[Figure 6 about here.]

The surface model layer (top 10 m) accounts for less than 5% of the full water column tracer content and masks significant features at depth. Depth-integrals of the tracers in Figure 6 show that while surface freshwater is

concentrated around the north of GVIIS and Alexander Island, the signals from surface inputs summed over all depths gather in Eltanin Bay. This occurs because the model predicts strong ice growth and convection in wintertime polynyas in this region (Holland et al., 2010), which mix the surface tracers down through the water column. Convection does not reach the sea bed, so the model is consistent with observations of a warm CDW layer in this region (Zhang et al., 2016). However, this deep mixed layer is unverified by observations and could be unrealistically deep.

The vertically-integrated tracers show that ice-shelf melting (Figure 6f) is the largest contributor to freshwater over the full water column. At both ends of GVIIS, the vertically integrated ice shelf meltwater shows a strong enhancement, and this water is also able to reach the surface ocean in the north (Figure 5f).

The structure can be seen in vertical sections through Ronne Entrance (Figure 7) and Marguerite Trough (Figure 8). In Ronne Entrance, the surface layers are stratified with high levels of freshwater due to the surface inputs, with prescribed iceberg melt highest near the coast and evaporation and precipitation having more influence further across the shelf. A sub-surface layer of brine-enhanced water (Figure 7e) traces the deeper winter water from sea ice formation; the magnitude of this exceeds 0.5% offshore. The sea ice tracer has more influence at depth than the tracers of other surface inputs, though they counter its influence in the total freshwater content. Close to the coast, ice shelf meltwater dominates the intermediate depths down to 400 metres, the bulk of which remains at depth below the sea ice signal as its salinity is higher than the surface layers, resulting in a second area of high

freshwater concentration.

In Marguerite Trough (Figure 8), stratification of meltwater-enriched surface layers extends to the shelf break, but high levels of sea ice and ice shelf meltwater dominate at the ice shelf front. Ice shelf meltwater is able to reach the surface due to it being fresher than the meltwater in Ronne Entrance (Figure 7f) and the ambient water. The concentration of sea-ice brine-enhanced water is lower in Marguerite Trough than in Ronne Entrance, and the surface sea ice meltwater is stronger.

[Figure 7 about here.]

[Figure 8 about here.]

The sea ice tracer shows a strong vertical gradient, with a large positive tracer concentration at the surface everywhere except in Eltanin Bay (Figure 5e) and a larger volume of brine-enhanced water at depth (Figure 6e). With the simulations starting from zero sea ice tracer, positive meltwater fluxes are added to the surface in spring, and negative fluxes are extracted over a greater depth in autumn. This gradually forms the vertical structure in the model. We ascribe the overall dominance of negative tracer values (Figure 6e) to both the preferential export of surface meltwater out of the domain by the coastal current, and sea ice drift.

3.3. Freshwater seasonality

[Figure 9 about here.]

On an annual mean, the magnitude of freshwater fluxes and their associated tracers are comparable. However, the seasonal variation differs markedly

between tracers. The salinity at the surface, which receives the majority of freshwater inputs, has a strong seasonal cycle (Figure 9). The freshest waters occur in the summer and near to the coast, extending out to the shelf break, and to a lesser extent out to the maximum extent near 64 °S. Spring and autumn have similar salinity distributions, freshest in the north where there are multiple freshwater inputs. In the winter there is a net salinification in Eltanin Bay, which is also seen on a small scale in autumn and remains in spring.

[Figure 10 about here.]

The seasonal distribution of salinity (Figure 9) largely mirrors the distribution of the sea ice tracer (Figure 10). The autumn and spring sea ice tracers highlight the dominance of freezing in Eltanin Bay, and a large amount of melt remains close to Alexander Island late into autumn. High meltwater content in summer is offset by freezing in winter, providing opposing signals that partly compensate on an annual mean, dependent on the effect of the mixed layer depth. However, while sea ice tracer content has the most extreme magnitude in summer and winter (Figure 10), the sea ice freshwater flux is maximised in spring and autumn (Figure 11). Precipitation also shows seasonal variation in the form of a larger freshwater input in autumn than spring that extends further south to Marguerite Bay, especially close to the peninsula. This is not cancelled by evaporation (not shown). Glacial freshwater sources (ice shelf melt and prescribed iceberg melt) are seasonally uniform; the dominant ice shelf meltwater contribution from GVIIS displays little variability, and no data is available to suggest a seasonal cycle of iceberg melt in the BS is significant.

[Figure 11 about here.]

[Figure 12 about here.]

The seasonality of the spatially variable fluxes and tracers results in a strong seasonal cycle of salinity at different depths on the shelf (Figure 12). In winter, the upper ocean has relatively uniform salinity due to the deepened mixed layer (Figure 12a). The onset of surface freshening occurs in October, with the minimum salinity occurring in January. At deeper levels the lowest salinities occur later in summer following the onset of the deepening mixed layer, and are less pronounced.

The annual average, seasonal variability, and interannual variability of each component are quantified in Table 2.

[Table 2 about here.]

The seasonal cycle in the sea ice flux is an order of magnitude larger than seasonal variation in other freshwater inputs (Figure 12b, Table 2). Precipitation and evaporation peak in summer, once sea ice has melted. While their seasonal variability is higher than glacial inputs, their annual mean contribution is comparable.

The domination of sea ice variability on the seasonal flux cycle (Figure 12b) is reflected in the seasonality of its associated tracer concentration (Figure 12c). But while instantaneous freshwater fluxes are dominated by sea ice, the annual-mean flux, and hence the total freshwater concentration, is a balance of all sources. Table 2 shows that precipitation is the biggest annual contributor, followed by ice shelf meltwater flux, with sea ice contributing the least, negative due to seasonal refreezing. The associated precipitation and

ice shelf tracers are similarly large, with ice shelf melt dominating as shown earlier. The sea ice tracer content has a negative sign due to net freezing that overrides the strong positive signal from surface meltwater, indicating a high residence time of the subsurface brine-enhanced saline waters gained through seasonality of the mixed layer depth. The seasonal variability in freshwater tracers is lagged from the variability in its sources, with the peak sea ice and total freshwater tracer in February-March and peak precipitation tracer in June.

4. Interannual variability and trends

4.1. Variability

To investigate the temporal variability of freshwater on the shelf, the mean seasonal cycle has been removed to provide a timeseries of anomalies, shown as annual averages in Figures 12d-12f. Salinity in the top 100 metres shows interannual variability (Figure 12d), while deeper layers show little deviation from the mean.

While the seasonal cycle of sea ice flux is an order of magnitude larger than the other freshwater sources (Figure 12b), the interannual anomaly of both sea ice and precipitation flux are dominant, exceeding ten times and five times that of the least variable (Figure 12e; Table 2). The dominance of these in flux anomalies is apparent to a lesser extent in interannual variability of tracer content, with ice shelf melt and iceberg melt displaying more interannual variability than their associated fluxes (Table 2).

Anomalies in flux lead to changes in tracer content (Figure 12f). High sea ice melt tracer in 1989-1990 dominates the total freshwater tracer. This

is followed by a period of low total freshwater tracer due to low precipitation freshwater content in 1992-1995. From 1995, lower than average sea ice melt tracer broadly increases until 2006, where it remains higher than average until 2012. From 2006 the precipitation and ice shelf melt help to sustain high total freshwater content. After 2011 the model freshwater content dramatically decreases due to a large decrease in sea ice meltwater, despite an increase in freshwater content from precipitation and iceberg melt. The total freshwater tracer is mirrored by salinity at the surface (Figure 12d). In general, sea ice is the strongest contributor to variability in both total freshwater flux and total tracer, with a correlation of over 0.8 at the 99% significance level (Table 2); where there is a large difference this is due to precipitation offsetting the sea ice signal (Figure 12e,f).

4.2. Trends

Linear trends in salinity and freshwater tracers on the BS shelf are shown in Table 3. Over the full time period (1989-2014) there are no significant trends in salinity over most of the water column. However, there are compensating trends in the individual freshwater components. The precipitation flux from ERA-Interim in the model increases over time, as in observations (Thomas et al., 2008), contributing to more precipitation tracer on the shelf (Figure 12f). Significantly, the iceberg melt tracer increases over the model period despite having a constant prescribed flux, showing that ocean dynamics are paramount; the input flux outweighs export from the shelf during this period. This is probably due to meltwater accumulation in regions with a long residence time, such as Eltanin Bay (Figure 6), and could have subsequent effects on the seasonal Antarctic Peninsula Coastal

Current (Moffat et al., 2008). Ice shelf meltwater content has an insignificant trend, despite observations suggesting an increase in melting in recent years in the area (Paolo et al., 2015).

[Table 3 about here.]

The dominant feature in both the surface salinity and freshwater tracers is a surface freshening from 1992-2011 (Figures 12d and 12f) which can be largely attributed to an increase in freshwater tracer from sea ice. Table 3 also shows the linear trends in all components during this shorter time period. It should be noted here that the anomalously low salinity in 2011 does partially drive the 1992-2011 trend. However, apart from surface salinity, trends that occurred in 1992-2011 remain if looking at 1992-2010, albeit to a smaller extent. We now focus on the strong changes occurring during this period because 1) it enables comparison with the many previous studies that have examined these changes, and 2) it provides a case study of strong decadal freshwater change.

The tracers associated with precipitation, evaporation, and iceberg melting show significant changes in freshwater from 1989-2014, but their sum does not create significant freshening at the surface. Over 1992-2011, however, the clear freshening can be attributed to significant increases in freshwater tracers, of which iceberg melt, evaporation and sea ice melt are significant contributors at the 95% level (Table 3). Increases in precipitation and ice shelf melting also contribute to the freshening, albeit significant at only the 90% level. The main difference is sea ice; an increase in sea ice tracer contributes over half the total freshwater trend in 1992-2011, but has no significant trend over the whole model period.

Figure 13 shows the seasonal trends in sea ice concentration from observations (Cavalieri et al., 1996) over the full time period 1989-2014, and the identified period of increased melting 1992-2011. A loss of sea ice is observed over both time periods in summer and autumn. In winter and spring, however, 1989-2014 shows an increase in sea ice while 1992-2011 shows a general ice loss. The strong summer-intensified ice loss from the BS (Holland, 2014) is robust for all time periods but during 1989-2014 there is no annual-mean trend because winter ice gain offsets summer ice loss.

Figure 14 shows the modelled sea ice concentration, drift, thickness, and freshwater flux trends over the period of increased sea ice freshwater 1992-2011. Comparing the model to observations (Figure 13) shows that overall ice concentration trends are very generally captured, though the model ice loss is not focused on the coastline, and little ice exists in summer. Whilst summer and autumn losses are recreated, the loss in winter and spring is not. In any model forced by coarse reanalysis winds, we can only expect to reproduce the broad features of complex regional changes such as these, which is sufficient for our shelf-wide analysis of freshwater trends.

The 1992-2011 freshening can be explained by trends in seasonal ice motion and thickness (Figure 14). In autumn and winter, reduced sea ice extent across the BS is caused by strong northerly wind trends forcing the sea ice towards the BS coast, resulting in ice thinning in the north and thickening at the southern coastline (Holland et al., 2014), as shown in the thickness and velocity vector trends of Figure 14. This wind-driven change is accompanied by a significant reduction in freezing in autumn on the northern BS shelf, and consequently a reduction in autumn and winter ice concentration and

thickness. It is this reduction in brine rejection on the shelf that causes the increase in annual-mean sea ice freshwater content (Table 3). This is at odds with Meredith and King (2005) (hereafter MK), who find that observed decreasing autumn sea ice production results in saltier surface layers. However, MK find significant salinification in the north, which both contains off-shelf waters and does not account for southern changes as in our calculations. Additionally, the time period of observations is different to this study.

MK use a simple 1D column model to argue that increased ice production leads to increased meltwater input in summer and thus a fresher surface layer. Thus their observed trend to higher summer salinity is consistent with reduced ice production. The present paper concludes that a year-round freshening is caused by reduced ice production. The two arguments may at first appear contradictory. However, the sole intention of the MK model was to consider the seasonality in the impact of a given annual-mean ice anomaly. That study compared simulations with two different values of a fixed repeating cycle in ice production. By contrast, the present study considers interannual trends in the annual-mean ocean salinity, driven by a progressively evolving annual-mean ice production. The present study also considers freshwater forcings other than sea ice, and is fully conservative in three dimensions. Thus the MK model explains the expected seasonality of trends in an idealised setting, while the present study explains the magnitude of annual-mean trends in a more realistic scenario.

[Figure 13 about here.]

[Figure 14 about here.]

5. Conclusions

This study uses a numerical model equipped with freshwater tracers to derive a freshwater budget of the Bellingshausen Sea. We find that sea ice dominates the seasonal freshwater cycle such that sea ice fluxes are instantaneously an order of magnitude larger than any other source. However, on an annual mean, all fluxes (precipitation, evaporation, sea ice, icebergs and ice shelves) are comparable, while sea ice and precipitation dominate interannual variability and trends. The on-shelf content of each tracer largely reflects this also, though the dominance of sea ice tracer in the seasonal cycle is dampened. Each component has its own temporal and spatial variability, and none can be neglected a priori. Ice shelf melt is the largest single contributor to mean freshwater content in the BS, thus it is vital that its contribution is further understood in light of recent changes to ice shelf melting. This is particularly key for isotopic analysis, where high meteoric water content in some areas (e.g. Meredith et al., 2013) is not able to be attributed to individual sources.

Ice shelf melt is less pronounced in the surface despite being the dominant contributor over the whole water column. South of George VI Ice Shelf, the peak ice shelf meltwater resides at intermediate depths, while to the north it reaches the surface, agreeing well with Jenkins and Jacobs (2008). This result has important implications for the interpretation, and comparison, of geographically-separated sediment core δ^{18}O records that may be recording waters from different sources, or missing the bulk of some freshwater components, despite the δ^{18}O being measured on organisms living at the same depth and in the same ecological niche. While it confirms the presence of ice

shelf meltwater in the north away from its source, as inferred from sediment cores (e.g. Pike et al., 2013), it suggests deeper meltwater content may be missed.

Seasonal and spatial variation in freshwater fields can be hidden by sparsity of data. In Eltanin Bay, strong winter salinification from sea ice growth is masked by a net positive total freshwater content from meteoric sources, showing the importance of identifying the full regional composition of freshwater. Additionally, when assessing the freshwater balance, the different origins of freshwater content cannot be deduced from fluxes, or vice versa, since many freshwater constituents are far removed in space and time from their sources.

Over the full model period (1989-2014) there are no overall salinity trends despite increasing precipitation, evaporation, and iceberg melt tracers (the latter increasing despite a constant prescribed flux). Ocean observations are insufficient to determine whether any salinity trends occurred in reality during this period, though some components of the freshwater budget clearly changed (e.g. Parkinson and Cavalieri, 2012; Wouters et al., 2015). However, a strong surface freshening occurs during 1992-2011, a period studied by several previous authors (e.g. Parkinson and Cavalieri (2012); Holland and Kwok (2012); Holland et al. (2014)). In our model, a strong decrease in ice growth in autumn causes this freshening, driven by northerly wind trends. This illustrates the importance of sea ice to decadal freshwater change.

One of the main limitations of this study is the use of a spatially and temporally uniform composite runoff field, representing liquid runoff, ice front melting, and iceberg melt. Given the significance of freshwater injec-

tion depth on water column stability, prescribing iceberg melting in surface coastal areas is likely to miss important features in the Bellingshausen Sea freshwater composition. Another significant limitation is that the sparsity of observations of freshwater content in the polar regions means that such models of freshwater processes cannot be fully validated. This is particularly relevant given the reasonably low resolution of the model at the coast which is likely to affect freshwater fields in those areas, particularly precipitation which originates from a coarse dataset that therefore may not fully resolve the effects of the AP mountains. The large spatial and temporal variation of our modelled tracers highlight the need for dedicated δ^{18}O observations to complement modelling efforts in order to understand the relative importance of each freshwater source.

6. Acknowledgements

This work was funded through a NERC DTG studentship (Project Reference: NE/L501633/1) to the British Antarctic Survey. This paper is a contribution of the BAS Polar Oceans programme. We thank Melchior van Wessem and colleagues at the Institute for Marine and Atmospheric Research Utrecht for providing data for use in computing the iceberg melt field. The MITgcm model is an open source model (mitgcm.org) and was forced with data as described in the methods section.

Cavalieri, D.J., Parkinson, C.L., Gloerson, P., Zwally, H.J., 1996. Sea Ice Concentrations from Nimbus-7 SMMR and DMSP SSM/I-SSMIS Passive Microwave Data, Version 1. [1989-2014] *digital media*. NASA DAAC at the National Snow and Ice Data Center, Boulder, Colorado USA.

633 Cook, A.J., Fox, A.J., Vaughan, D.G., Ferrigno, J.G., 2005. Retreating
634 glacier fronts on the Antarctic Peninsula over the past half-century. Science
635 308, 541–544.

636 Cook, A.J., Holland, P.R., Meredith, M.P., Murray, T., Luckman, A.,
637 Vaughan, D.G., 2016. Ocean forcing of glacier retreat in the western
638 Antarctic Peninsula. Science 353, 283–286.

639 De Rydt, J., Holland, P.R., Dutrieux, P., Jenkins, A., 2014. Geometric and
640 oceanographic controls on melting beneath Pine Island Glacier. Journal of
641 Geophysical Research: Oceans 119, 2420–2438.

642 Dee, D.P., Uppala, S.M., Simmons, A.J., Berrisford, P., Poli, P., Kobayashi,
643 S., Andrae, U., Balmaseda, M.A., Balsamo, G., Bauer, P., Bechtold, P.,
644 Beljaars, A.C.M., van de Berg, L., Bidlot, J., Bormann, N., Delsol, C., Dra-
645 gani, R., Fuentes, M., Geer, A.J., Haimberger, L., Healy, S.B., Hersbach,
646 H., Hólm, E.V., Isaksen, L., Kållberg, P., Köhler, M., Matricardi, M.,
647 McNally, A.P., Monge-Sanz, B.M., Morcrette, J.J., Park, B.K., Peubey,
648 C., de Rosnay, P., Tavolato, C., Thépaut, J.N., Vitart, F., 2011. The
649 ERA-Interim reanalysis: Configuration and performance of the data as-
650 similation system. Quarterly Journal of the Royal Meteorological Society
651 137, 553–597.

652 Depoorter, M.A., Bamber, J.L., Griggs, J.A., Lenaerts, J.T.M., Ligtenberg,
653 S.R.M., van den Broeke, M.R., Moholdt, G., 2013. Calving fluxes and
654 basal melt rates of Antarctic ice shelves. Nature 502, 89–92.

655 Dierssen, H.M., Smith, R.C., Vernet, M., 2002. Glacial meltwater dynamics

in coastal waters west of the Antarctic Peninsula. Proceedings of the National Academy of Sciences of the United States of America 99, 1790–1795.

Dinniman, M.S., Klinck, J.M., Hofmann, E.E., 2012. Sensitivity of Circumpolar Deep Water Transport and Ice Shelf Basal Melt along the West Antarctic Peninsula to Changes in the Winds. Journal of Climate 25, 4799–4816.

Fretwell, P., Pritchard, H.D., Vaughan, D.G., Bamber, J.L., Barrand, N.E., Bell, R., Bianchi, C., Bingham, R.G., Blankenship, D.D., Casassa, G., Catania, G., Callens, D., Conway, H., Cook, A.J., Corr, H.F.J., Damaske, D., Damm, V., Ferraccioli, F., Forsberg, R., Fujita, S., Gim, Y., Gogineni, P., Griggs, J.A., Hindmarsh, R.C.A., Holmlund, P., Holt, J.W., Jacobel, R.W., Jenkins, A., Jokat, W., Jordan, T., King, E.C., Kohler, J., Krabill, W., Riger-Kusk, M., Langley, K.A., Leitchenkov, G., Leuschen, C., Luyendyk, B.P., Matsuoka, K., Mouginot, J., Nitsche, F.O., Nogi, Y., Nost, O.A., Popov, S.V., Rignot, E., Rippin, D.M., Rivera, A., Roberts, J., Ross, N., Siegert, M.J., Smith, A.M., Steinhage, D., Studinger, M., Sun, B., Tinto, B.K., Welch, B.C., Wilson, D., Young, D.A., Xiangbin, C., Zirizzotti, A., 2013. Bedmap2: Improved ice bed, surface and thickness datasets for Antarctica. Cryosphere 7, 375–393.

Graham, J.A., Dinniman, M.S., Klinck, J.M., 2016. Impact of model resolution for on-shelf heat transport along the west Antarctic Peninsula. Journal of Geophysical Research: Oceans 121, 7880–7897.

679 Hellmer, H.H., 2004. Impact of Antarctic ice shelf basal melting on sea ice
680 and deep ocean properties. Geophysical Research Letters 31, L10307.

681 Holland, D.M., Jenkins, A., 1999. Modeling Thermodynamic Ice-Ocean In-
682 teractions at the Base of an Ice Shelf. Journal of Physical Oceanography
683 29, 1787–1800.

684 Holland, P.R., 2014. The seasonality of Antarctic sea ice trends. Geophysical
685 Research Letters 41, 4230–4237.

686 Holland, P.R., Bruneau, N., Enright, C., Losch, M., Kurtz, N., Kwok, R.,
687 2014. Modelled trends in Antarctic sea ice thickness. Journal of Climate
688 27, 3784–3801.

689 Holland, P.R., Jenkins, A., Holland, D.M., 2010. Ice and ocean processes in
690 the Bellingshausen Sea, Antarctica. Journal of Geophysical Research 115,
691 C05020.

692 Holland, P.R., Kimura, N., 2016. Observed concentration budgets of Arctic
693 and Antarctic sea ice. Journal of Climate 29, 5241–5249.

694 Holland, P.R., Kwok, R., 2012. Wind-driven trends in Antarctic sea-ice drift.
695 Nature Geoscience 5, 872–875.

696 Jenkins, A., Jacobs, S., 2008. Circulation and melting beneath George VI
697 Ice Shelf, Antarctica. Journal of Geophysical Research 113, C04013.

698 Klinck, J.M., Hofmann, E.E., Beardsley, R.C., Salihoglu, B., Howard, S.,
699 2004. Water-mass properties and circulation on the west Antarctic Penin-

sula continental shelf in austral fall and winter 2001. Deep Sea Research Part II: Topical Studies in Oceanography 51, 1925–1946.

Martinson, D.G., Stammerjohn, S.E., Iannuzzi, R.A., Smith, R.C., Vernet, M., 2008. Western Antarctic Peninsula physical oceanography and spatio-temporal variability. Deep Sea Research Part II: Topical Studies in Oceanography 55, 1964–1987.

Meredith, M.P., Brandon, M.A., Wallace, M.I., Clarke, A., Leng, M.J., Renfrew, I.a., van Lipzig, N.P., King, J.C., 2008. Variability in the freshwater balance of northern Marguerite Bay, Antarctic Peninsula: Results from δ^{18}O. Deep Sea Research Part II: Topical Studies in Oceanography 55, 309–322.

Meredith, M.P., King, J.C., 2005. Rapid climate change in the ocean west of the Antarctic Peninsula during the second half of the 20th century. Geophysical Research Letters 32, L19604.

Meredith, M.P., Stammerjohn, S.E., Venables, H.J., Ducklow, H.W., Martinson, D.G., Iannuzzi, R.A., Leng, M.J., van Wessem, J.M., Reijmer, C.H., Barrand, N.E., 2016. Changing distributions of sea ice melt and meteoric water west of the Antarctic Peninsula. Deep-Sea Research Part II: Topical Studies in Oceanography .

Meredith, M.P., Venables, H.J., Clarke, A., Ducklow, H.W., Erickson, M., Leng, M.J., Lenaerts, J.T.M., Van Den Broeke, M.R., 2013. The freshwater system west of the Antarctic Peninsula: Spatial and temporal changes. Journal of Climate 26, 1669–1684.

723 Meredith, M.P., Wallace, M.I., Stammerjohn, S.E., Renfrew, I.A., Clarke, A.,
724 Venables, H.J., Shoosmith, D.R., Souster, T., Leng, M.J., 2010. Changes in
725 the freshwater composition of the upper ocean west of the Antarctic Penin-
726 sula during the first decade of the 21st century. Progress in Oceanography
727 87, 127–143.

728 Merino, I., Le Sommer, J., Durand, G., Jourdain, N.C., Madec, G., Mathiot,
729 P., Tournadre, J., 2016. Antarctic icebergs melt over the Southern Ocean:
730 climatology and impact on sea ice. Ocean Modelling 104, 99–110.

731 Moffat, C., Beardsley, R.C., Owens, B., van Lipzig, N., 2008. A first descrip-
732 tion of the Antarctic Peninsula Coastal Current. Deep Sea Research Part
733 II: Topical Studies in Oceanography 55, 277–293.

734 Nakayama, Y., Timmermann, R., Rodehacke, C.B., Schröder, M., Hellmer,
735 H.H., 2014. Modeling the spreading of glacial meltwater from the Amund-
736 sen and Bellingshausen seas. Geophysical Research Letters 41, 7942–7949.

737 Paolo, F.S., Fricker, H.A., Padman, L., 2015. Volume loss from Antarctic ice
738 shelves is accelerating. Science 348, 327–331.

739 Parkinson, C.L., Cavalieri, D.J., 2012. Antarctic sea ice variability and
740 trends, 1979-2010. The Cryosphere 6, 871–880.

741 Pike, J., Swann, G.E.A., Leng, M.J., Snelling, A.M., 2013. Glacial dis-
742 charge along the west Antarctic Peninsula during the Holocene. Nature
743 Geoscience 6, 199–202.

744 Pritchard, H.D., Vaughan, D.G., 2007. Widespread acceleration of tidewater

glaciers on the Antarctic Peninsula. Journal of Geophysical Research: Earth Surface 112, 1–10.

Regan, H., 2017. Modelling the sources, variability and fate of freshwater in the Bellingshausen Sea, Antarctica. PhD Thesis, Cardiff University, Cardiff, United Kingdom .

Rignot, E., Jacobs, S., Mouginot, J., Scheuchl, B., 2013. Ice-shelf melting around Antarctica. Science 341, 266–270.

Savidge, D.K., Amft, J.A., 2009. Circulation on the west Antarctic Peninsula derived from 6 years of shipboard ADCP transects. Deep Sea Research Part I: Oceanographic Research Papers 56, 1633–1655.

Stammerjohn, S., Massom, R., Rind, D., Martinson, D., 2012. Regions of rapid sea ice change : An inter-hemispheric seasonal comparison. Geophysical Research Letters 39, L06501.

Swann, G.E., Pike, J., Snelling, A.M., Leng, M.J., Williams, M.C., 2013. Seasonally resolved diatom δ^{18}O records from the West Antarctic Peninsula over the last deglaciation. Earth and Planetary Science Letters 364, 12–23.

Talley, L., 2011. Descriptive Physical Oceanography: An Introduction. Elsevier Science. 6 edition.

Thomas, E.R., Marshall, G.J., McConnell, J.R., 2008. A doubling in snow accumulation in the western Antarctic Peninsula since 1850. Geophysical Research Letters 35, 1–5.

766 Tournadre, J., Bouhier, N., Girard-Ardhuin, F., Rémy, F., 2015. Large ice-
767 bergs characteristics from altimeter waveforms analysis. Journal of Geo-
768 physical Research: Oceans 120, 1954–1974.

769 Turner, J., Lachlan-Cope, T., Colwell, S., Marshall, G.J., 2005b. A positive
770 trend in western Antarctic Peninsula precipitation over the last 50 years
771 reflecting regional and Antarctic-wide atmospheric circulation. Annals of
772 Glaciology 41, 85–91.

773 Turner, J., Lu, H., White, I., King, J.C., Phillips, T., Hosking, J.S., Brace-
774 girdle, T.J., Marshall, G.J., Mulvaney, R., Deb, P., 2016. Absence of 21st
775 century warming on Antarctic Peninsula consistent with natural variabil-
776 ity. Nature 535, 411–415.

777 van Wessem, J.M., Meredith, M.P., Reijmer, C.H., van den Broeke, M.R.,
778 Cook, A.J., 2016. Characteristics of the modelled meteoric freshwater
779 budget of the western Antarctic Peninsula. Deep Sea Research Part II:
780 Topical Studies in Oceanography .

781 Wouters, B., Martin-Espanol, A., Helm, V., Flament, T., van Wessem, J.M.,
782 Ligtenberg, S.R.M., van den Broeke, M.R., Bamber, J.L., 2015. Dynamic
783 thinning of glaciers on the southern Antarctic Peninsula. Science 348,
784 899–903.

785 Xie, H., Tekeli, A.E., Ackley, S.F., Yi, D., Zwally, H.J., 2013. Sea ice
786 thickness estimations from ICESat Altimetry over the Bellingshausen and
787 Amundsen seas, 2003-2009. Journal of Geophysical Research: Oceans 118,
788 2438–2453.

789 Zhang, X., Thompson, A.F., Flexas, M.M., Roquet, F., Bornemann, H.,
790 2016. Circulation and meltwater distribution in the Bellingshausen Sea:
791 From shelf break to coast. Geophysical Research Letters 43, 6402–6409.

List of changes

List of Figures

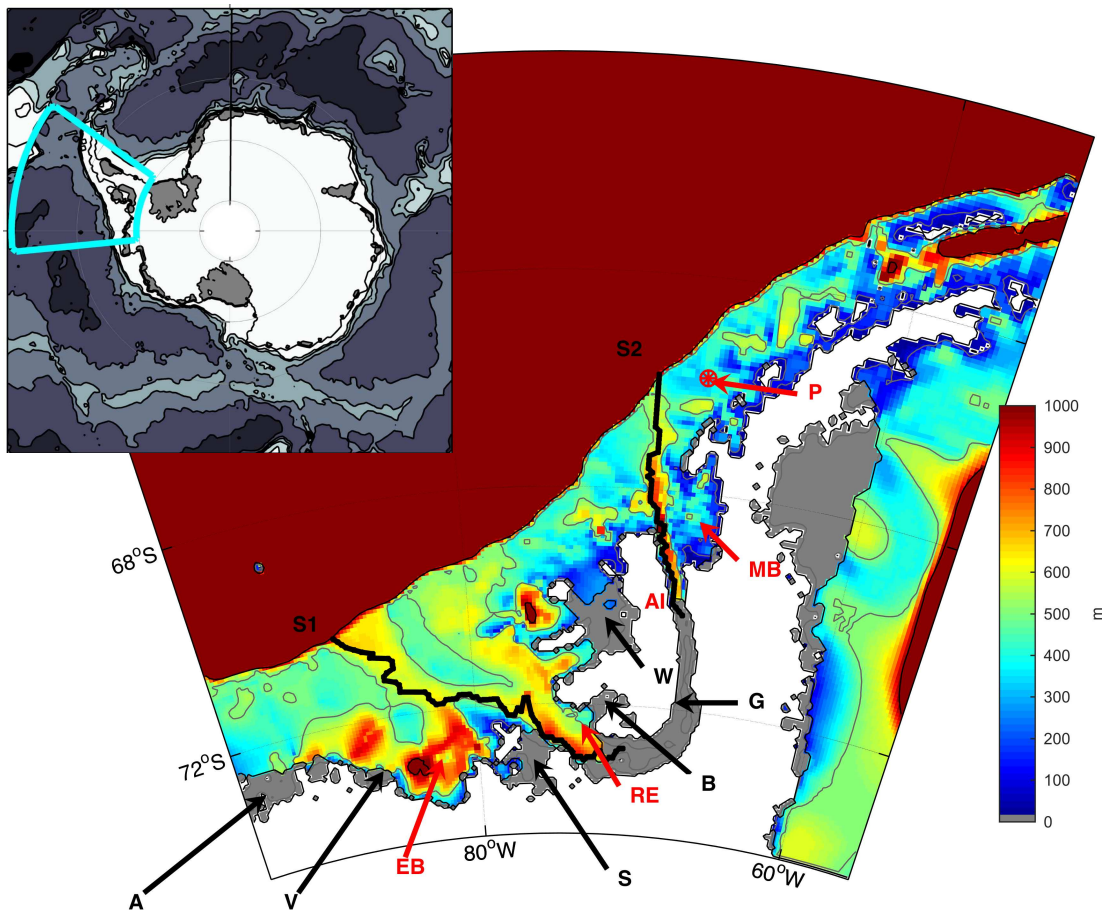

Figure 1: Model domain. Coloured is BEDMAP2 bathymetry, with contours shown at 100, 500, and 1000 metres. Ice shelves are shown in grey, with underlying bathymetry contours shown. Also provided in red are key locations, where EB = Eltanin Bay, RE = Ronne Entrance, AI = Alexander Island, MB = Marguerite Bay and P = Palmer LTER grid point 400.1, used for validation. Ice shelves on the west Antarctic Peninsula are shown with black arrows, where A = Abbot, V = Venable, S = Stange, B = Bach, W = Wilkins and G = George VI. Sections through Belgica Trough leading to Ronne Entrance (S1) and Marguerite Trough (S2) are also shown (black). Inset shows the Bellingshausen Sea and model domain (blue) in relation to the Southern Ocean and Antarctic Ice Sheet.

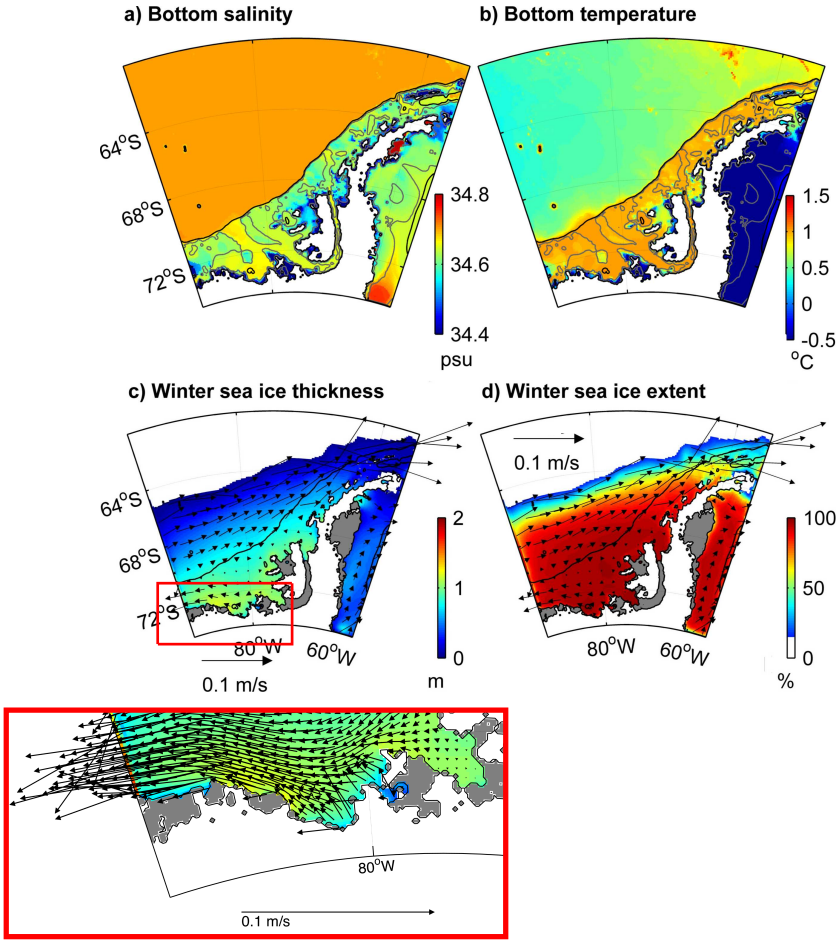

Figure 2: Annual mean a) salinity and b) potential temperature at the seabed for the period 1989-2014. Bathymetry contours shown in grey at 100, 500, and 1000 metres, with the 1000 metre isobath shown in black. Mean winter (JAS) sea ice thickness (c) and extent (d) is shown over the same period masked where sea ice concentration is below 15%, with ice shelves in grey. Vectors of ice velocity at 12 grid point intervals are also shown. Inset highlights the effect of the coastal current on the mean winter sea ice velocities.

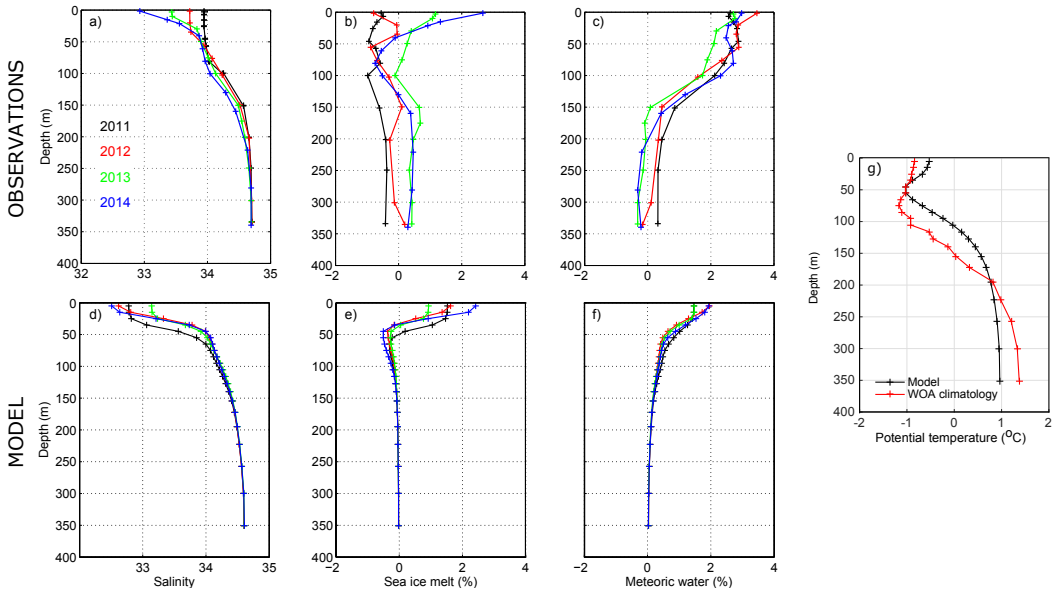

Figure 3: Salinity (a,d), sea ice melt (b,e) and meteoric water content (c,f) at 65°52.6' S, 68°17.0' W (see Figure 1). Top row (a-c) reproduced from Meredith et al. (2016) for validation purposes, with bottom row (d-f) showing the model equivalent for January 2011 (black), 2012 (red), 2013 (green) and 2014 (blue). Climatological potential temperature at the same location (g) is shown for the model (black, averaged over 1989-2014, after the spin-up period) and World Ocean Atlas data (red).

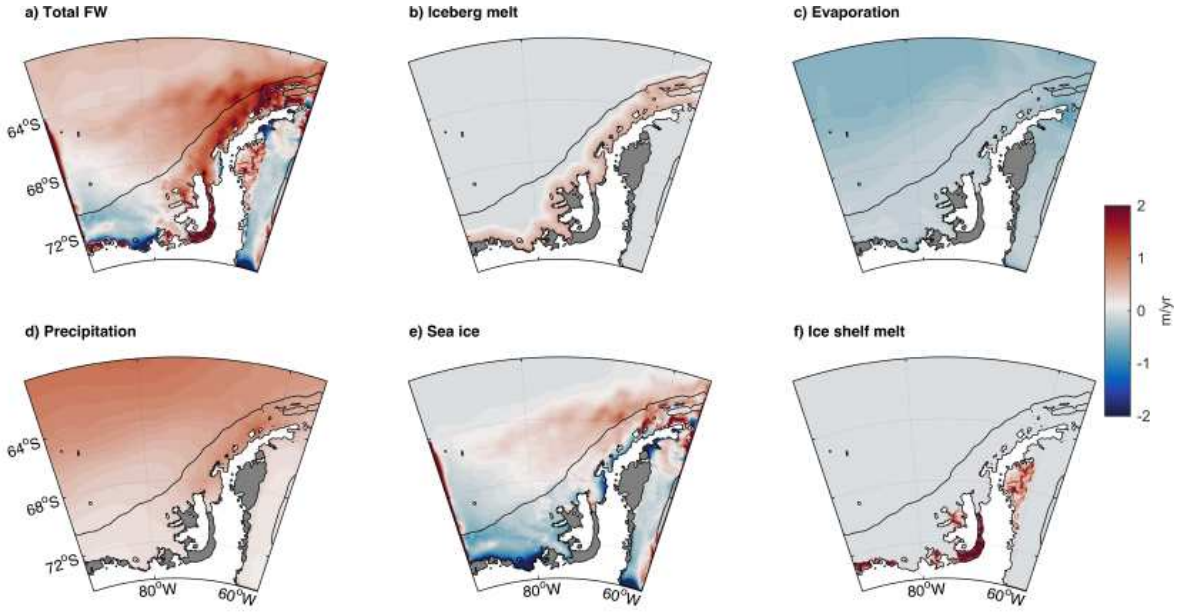

Figure 4: Climatology of freshwater fluxes at injection depth (positive downwards) for a) total freshwater, b) iceberg melt, c) evaporation, d) precipitation, e) sea ice and f) ice shelf melt, all shown on the same scale. Grey regions indicate ice shelves, with the shelf break contoured at 1000 metres.

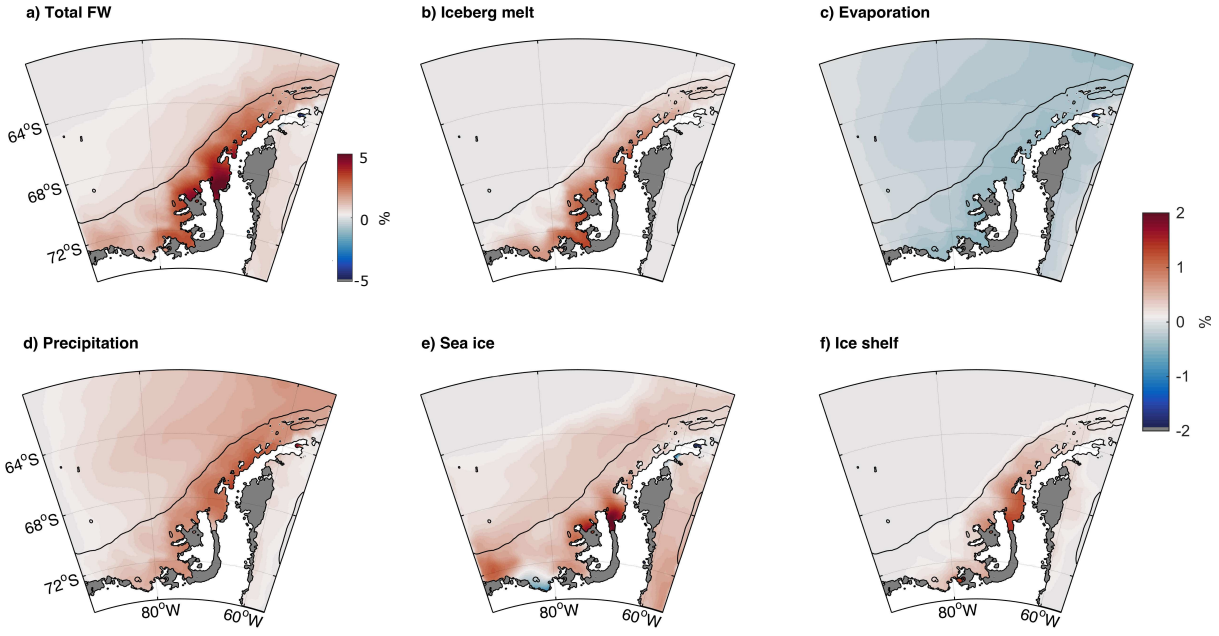

Figure 5: Climatological surface concentration of tracers from 1989-2014 for a) total freshwater, b) iceberg melt, c) evaporation, d) precipitation, e) sea ice and f) ice shelf melt. Grey regions indicate ice shelves, with the shelf break contoured at 1000 metres. Note the different colour scale for total freshwater.

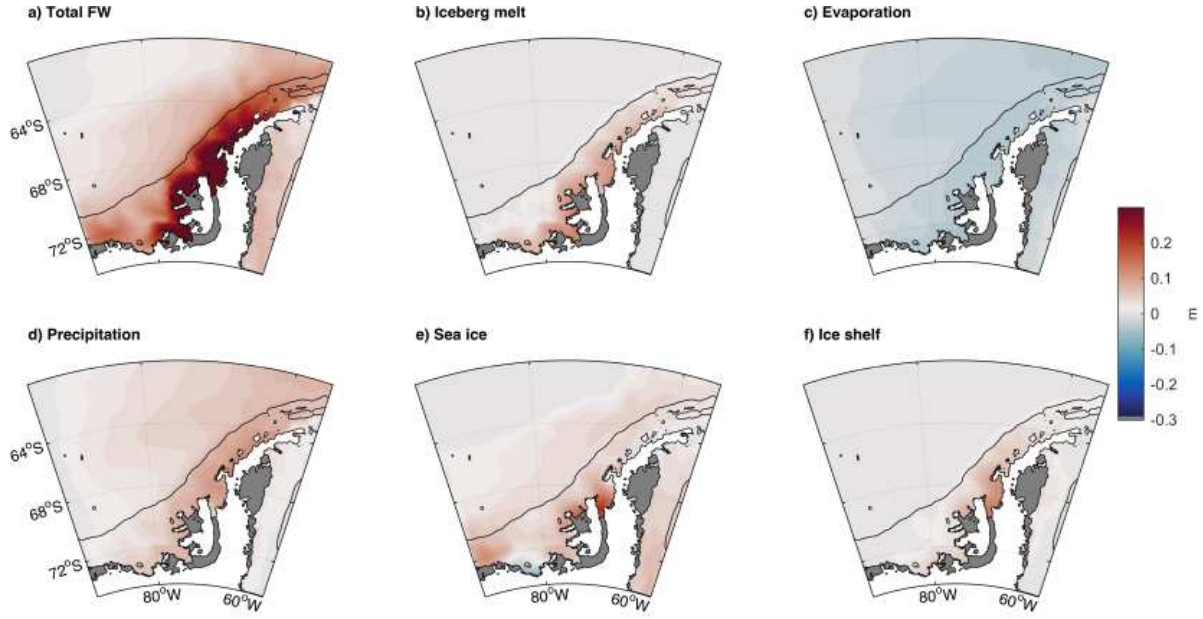

Figure 6: Climatological water-column integral of each tracer from 1989-2014, in metres. a) Total freshwater b) iceberg melt, c) evaporation, d) precipitation, e) sea ice and f) ice shelf melt all shown on the same scale. Bathymetry contours are shown at 100, 500, and 1000 metres.

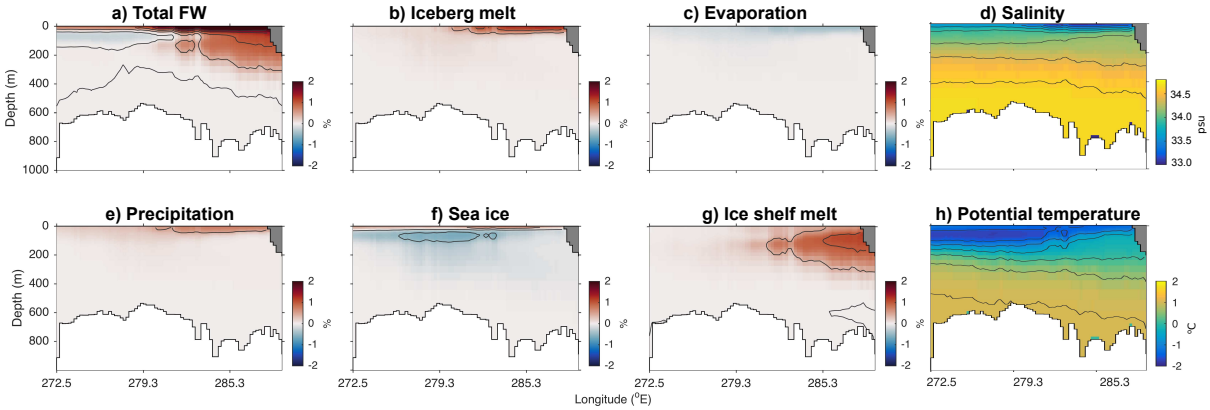

Figure 7: Vertical sections from the shelf break, through the deepest part of Belgica Trough from north-west to south-east through Ronne Entrance (S1 in Figure 1) for the climatology of a) total freshwater content, b) iceberg melt, c) evaporation, d) salinity, e) precipitation, f) sea ice, g) ice shelf melt, and h) potential temperature. Contours are shown at 0.5% intervals.

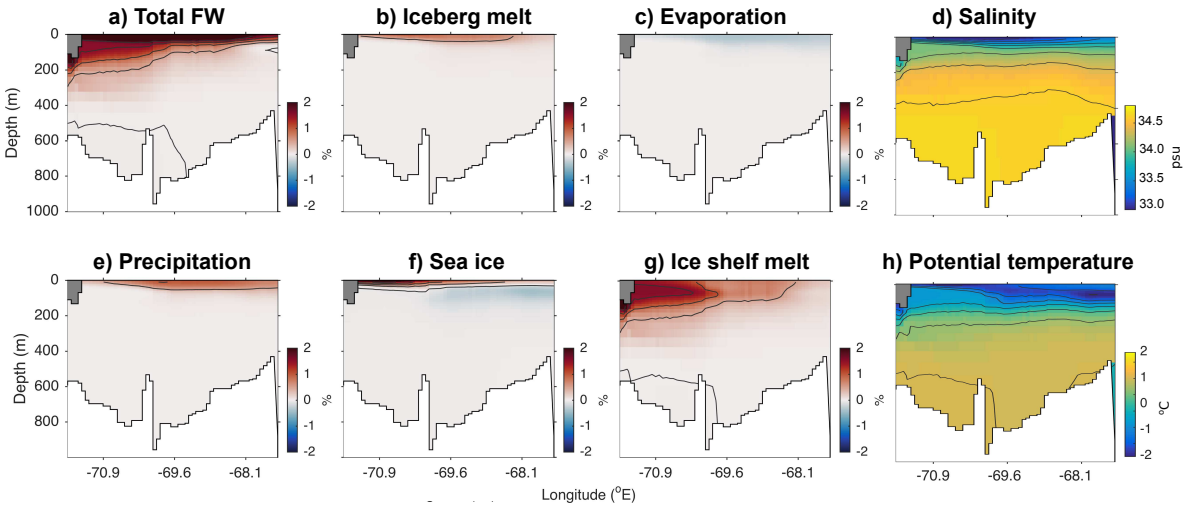

Figure 8: Vertical sections from George VI Ice Shelf through the deepest part of Marguerite Trough to the shelf break (S2 in Figure 1) for the climatology of a) total freshwater content, b) iceberg melt, c) evaporation, d) salinity, e) precipitation, f) sea ice, g) ice shelf melt, and h) potential temperature. Contours are shown at 0.5% intervals.

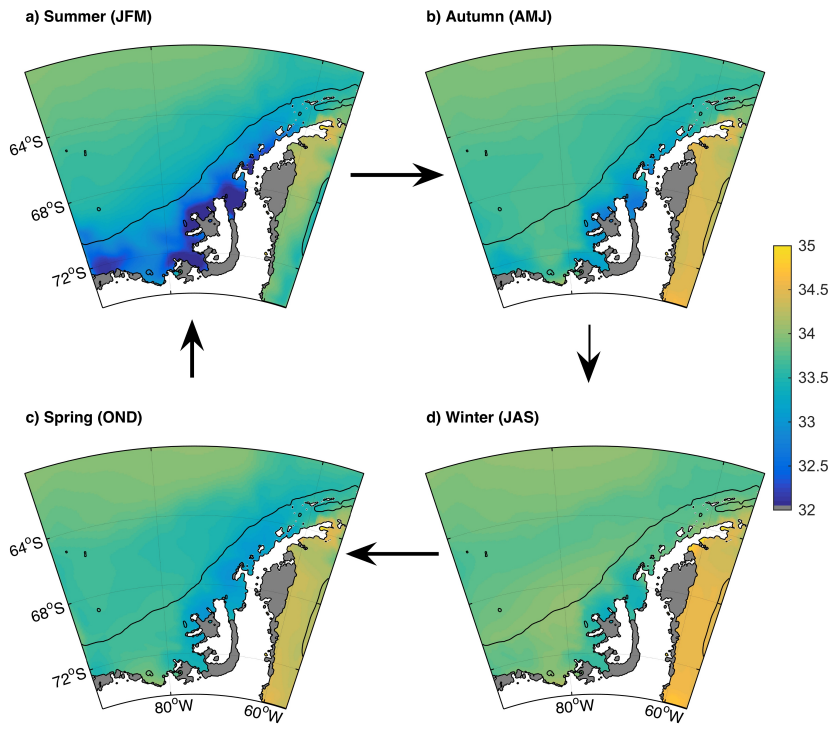

Figure 9: Average seasonal surface salinity, clockwise from top left: a) summer, b) autumn, d) winter and c) spring. Grey regions indicate ice shelves, with the shelf break contoured at 1000 metres.

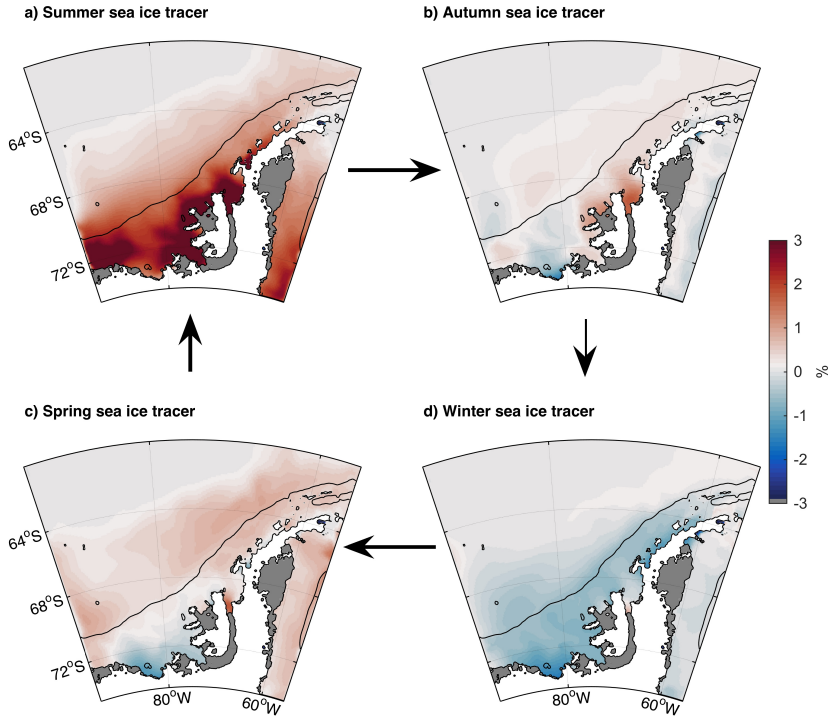

Figure 10: Seasonal distribution of sea ice tracer at the surface. Seasons are shown clockwise from top left: a) summer, b) autumn, d) winter and c) spring. Grey regions indicate ice shelves, with the shelf break contoured at 1000 metres.

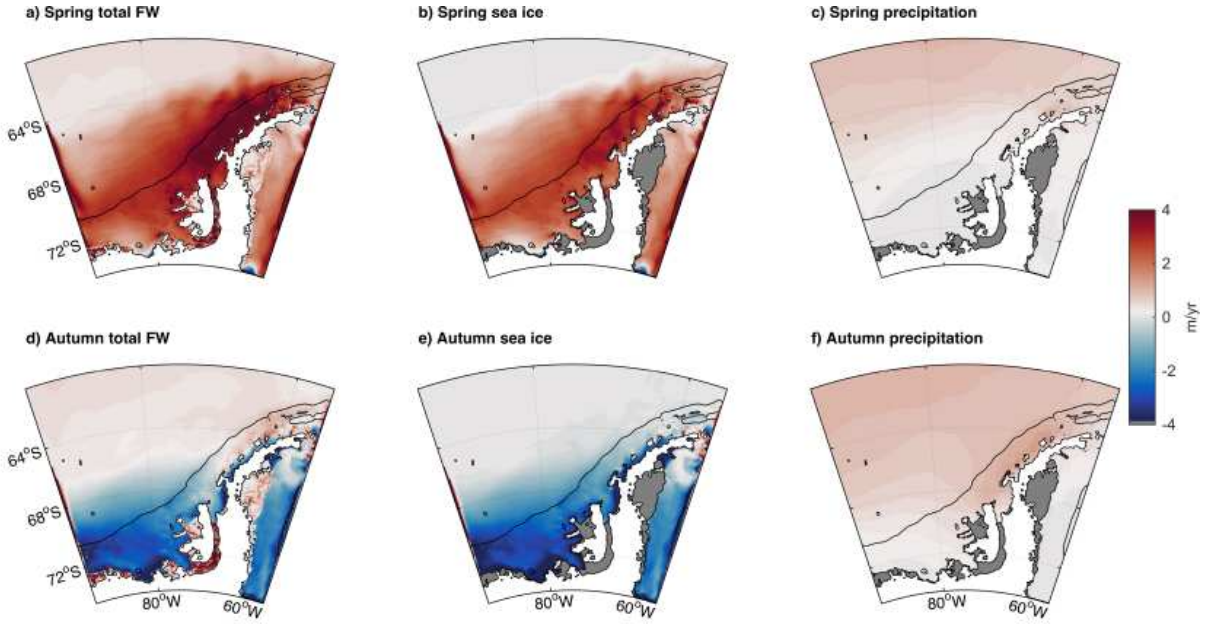

Figure 11: Seasonal distribution of fluxes of (a,d) total freshwater, (b,e) net sea ice melt/growth, and (c,f) precipitation for the spring (top) and autumn (bottom). Grey regions indicate ice shelves, with the shelf break contoured at 1000 metres.

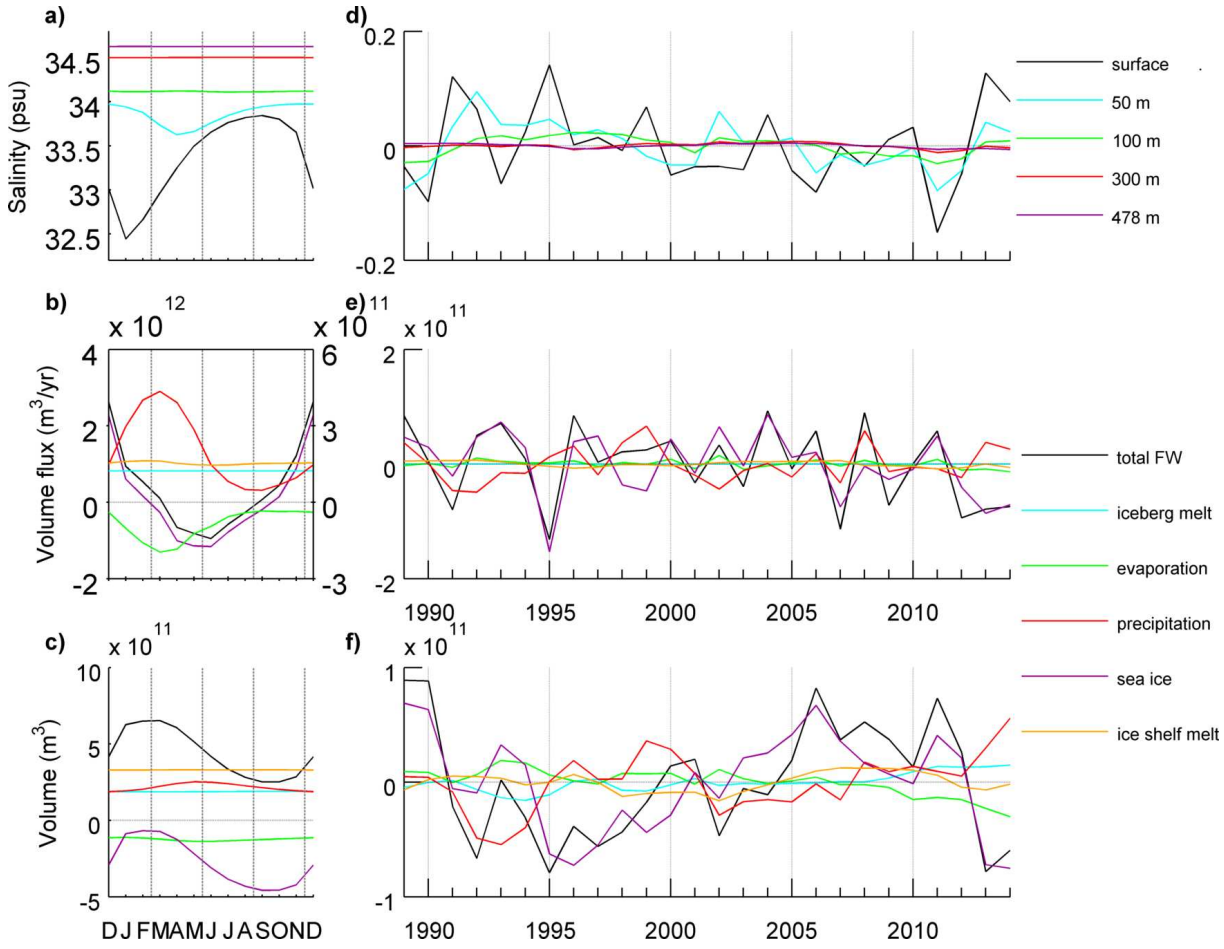

Figure 12: Temporal variation of freshwater on the BS shelf (shallower than 1000 metres). Plots on the left show (from top) seasonal cycles of a) mean salinity at different depths; b) area-integrated freshwater fluxes; and c) volume-integrated tracer content. Plots d)-f) on the right show the timeseries of deviations from the mean seasonal cycle, plotted as annual averages. Note the second y-axis in panel b) for iceberg melt, evaporation, precipitation and ice shelf melt.

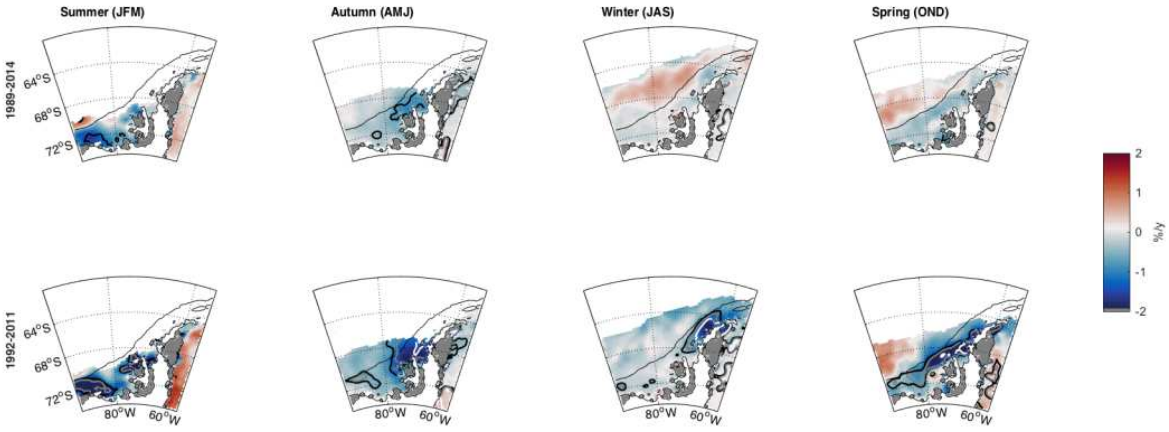

Figure 13: Trends of observed satellite-derived sea ice concentration from Cavalieri et al. (1996) for the full modelled period 1989-2014 (top) and period of increased sea ice flux, 1992-2011 (bottom). Confidence contours are shown at the 90% (black), 95% (grey) and 99% (white) levels. The shelf break is shown in black and ice shelves are in grey.

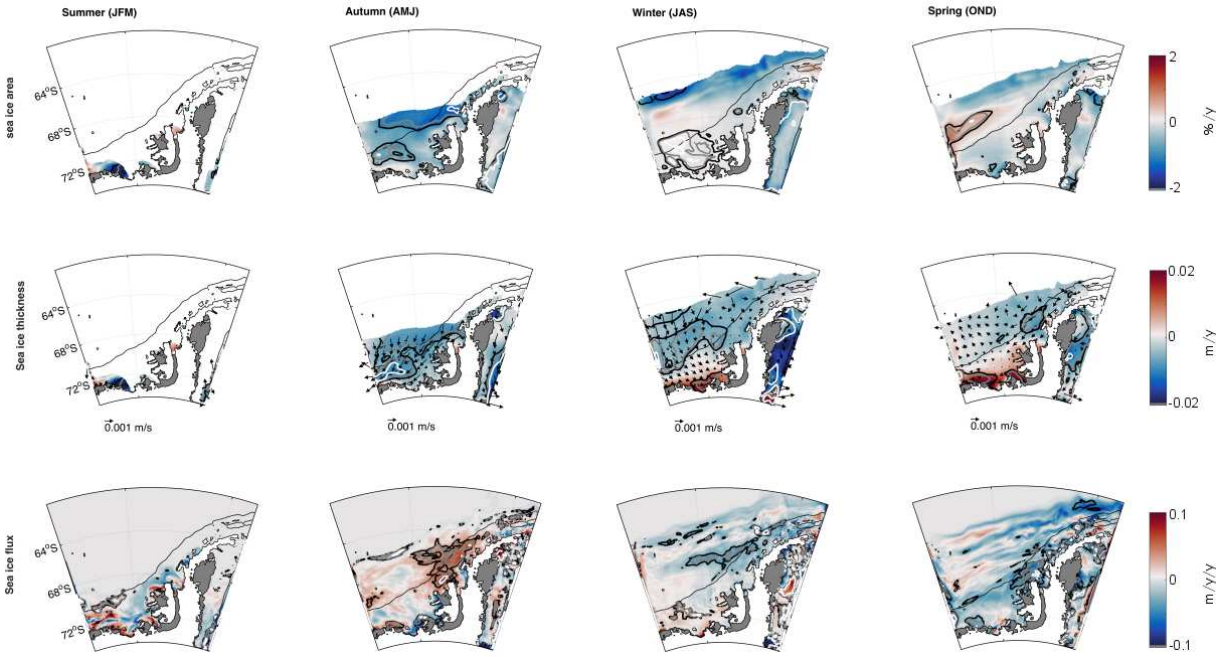

Figure 14: Modelled trends in sea ice area (top), thickness and drift (middle), and sea ice freshwater flux (bottom, positive downward) from 1992-2011. Confidence interval contours are shown at the 90% (black), 95% (grey) and 99% (white) levels. The shelf break is shown in black and ice shelves are in grey.

List of Tables

Table 1: Average ice shelf melt rates (m/yr) from the model are shown for the period 1989-2014, with error bars indicating 1 standard deviation of interannual variability. Also shown are the 2003-2008 average ice shelf melt rates from Rignot et al. (2013) and 1979-2010 melt rates from Depoorter et al. (2013) where available, with error bars showing observational error. Equivalent freshwater input in Gt/yr is also shown in brackets.

	Model (1989-2014)	Rignot *et. al.*, 2013 (2003-2008)	Depoorter *et. al.*, 2013 (1979-2010)
George VI	4.74±0.19	3.8±0.7	2.88±0.83
	(105.50±4.10)	(89±17)	(144±42)
Wilkins	1.00±0.28	1.5±1	-
	(13.07±3.80)	(18.4±17)	-
Bach	0.43±0.03	2.3±0.3	-
	(1.26±0.09)	(10.4±1)	-
Stange	1.11±0.26	3.5±0.7	-
	(9.08±2.20)	(28.0±6)	-
Venable	1.99±0.34	6.1±0.7	4.82±0.83
	(5.02±0.9)	(19.4±2)	(15±3)
Abbot	2.26±0.19	1.7±0.6	2.72±0.70
	(20.13±1.8)	(51.8±19)	(86±22)

Table 2: Table showing the annual mean, seasonal variability, interannual variability, and correlation against the total interannual timeseries for each flux (x 10^{11} m^3/y) and tracer (x 10^{11} m^3) on the shelf from Figure 12. The annual cycle was calculated by taking the average of each month over the 26 years, which was then averaged to produce the annual mean. Anomalies were calculated by removing the annual cycle from the timeseries, taking the yearly average and calculating the standard deviation of the result. Significance of correlation is indicated at the 90% (italic), 95% (bold) and 99% (bold, italic) levels.

	Annual mean	Seasonal variability (1 sd)	Interannual variability (1 sd)	Correlation
Total flux	2.11	10.26	0.67	*N/A*
Sea ice flux	-0.79	9.95	0.57	***0.82***
Precipitation flux	2.04	1.49	0.31	0.27
Evaporation flux	-0.92	0.61	0.07	**0.61**
Iceberg flux	1.23	*N/A*[o]	*N/A*[o]	*N/A*[o]
Ice shelf flux	1.53	0.06	0.05	0.09
Total tracer	4.41	1.62	0.51	*N/A*
Sea ice tracer	-2.77	1.57	0.44	***0.84***
Precipitation tracer	2.19	0.23	0.25	0.04
Evaporation tracer	-1.25	0.09	0.12	0.09
Iceberg tracer	1.89	0.01	0.08	0.13
Ice shelf tracer	3.30	0.01	0.08	0.36

[o]Not applicable as prescribed iceberg flux is temporally uniform

Table 3: Interannual trends in annual-mean anomaly from mean seasonal cycle shown for on-shelf salinity at various levels (y^{-1}), and in the total shelf tracer content (km^3y^{-1}). Trends are shown for the full time period and 1992-2011, identified as a period of freshening. Significance at the 90% (italic), 95% (bold) and 99% (bold, italic) confidence levels are indicated.

	1989-2014	1992-2011
Salinity (surface)	-0.0011	**-0.0047**
Salinity (50 m)	-0.0015	***-0.0051***
Salinity (100 m)	-0.0005	***-0.0020***
Salinity (300 m)	-0.0001	-0.0001
Salinity (478 m)	**-0.0002**	0.0000
Depth-averaged salinity	0.0004	***-0.0013***
Total tracer	0.50	***6.02***
Sea ice	-0.56	**3.39**
Precipitation	**1.50**	*1.68*
Evaporation	***-1.19***	***-1.10***
Iceberg	***0.78***	***0.93***
Ice shelf	0.18	*0.61*